A&A 485, 395–401 (2008)
DOI: 10.1051/0004-6361:200809499

Astronomy & Astrophysics

Optimising large galaxy surveys for ISW detection

M. Douspis[1], P. G. Castro[2], C. Caprini[3], and N. Aghanim[1]

[1] IAS CNRS, Bât. 121, Université Paris-Sud, 91405 Orsay, France
e-mail: [marian.douspis;nabila.aghanim]@ias.u-psud.fr
[2] CENTRA, Departamento de Física, Edifício Ciência, Piso 4, Instituto Superior Técnico, Av. Rovisco Pais 1, 1049-001 Lisboa, Portugal
e-mail: pgcastro@ist.utl.pt
[3] IPhT, CEA-Saclay, 91191 Gif-sur-Yvette, France
e-mail: chiara.caprini@cea.fr

Received 1 February 2008 / Accepted 4 March 2008

ABSTRACT

We investigate the potential of next-generation surveys of the cosmic microwave background and large-scale structure, to constrain the nature of dark energy, by means of the cross-correlation of the Integrated Sachs-Wolfe effect with the galaxy distribution. We first complete a signal-to-noise analysis to decide the most appropriate properties of a survey required to detect the correlated signal at a significance level of higher than 4σ. We find that more than 35% of the sky should be covered, the galaxy distribution should be probed out to a median redshift higher than 0.8, and the number of galaxies detected should be higher than a few per squared arcmin. We then consider in particular forthcoming surveys DUNE, LSST, SNAP, PanSTARRS. We independently compute the constraints that the DUNE survey can place on the nature of dark energy, by means of different parametrisations of its equation of state, using a standard Fisher matrix analysis. We confirm that, with respect to limits placed by pure CMB, cross-correlation constraints can help to break the degeneracies between dark energy and cosmological parameters. The strength of the constraints is not, of course, independent of the dark-energy model. The constraints are complementary to, despite being weaker than, some other probes of dark energy such as gravitational weak-lensing, because they are sensitive to the high-redshift behaviour of the dark energy.

Key words. surveys – cosmology: cosmic microwave background – cosmology: cosmological parameters

1. Introduction

Measurements of the Cosmic Microwave Background (CMB) angular power spectra are invaluable observables for constraining cosmology. The detailed shape of these spectra allows cosmological parameters to be determined with high precision. The "concordance" model, which has been developed over a number of years using observational data of the CMB, supernovae of type Ia, and galaxy distributions, appears to reproduce most cosmological observables well. This model requires the existence of a dark-energy component that can be described by a cosmological constant Λ. However, more complex scenarios cannot be ruled out by present datasets. Among them, one could imagine a dark-energy component with an equation of state w that is different from $w = -1$, which corresponds to a cosmological constant, or even varying in time $w(z)$, such as in scalar field quintessence models. Moreover, the effect of dark energy, which is a recent phase of accelerated expansion, could be mimicked by a deviation from standard gravity on large scales.

To achieve a more robust constraint and understanding of the present expansion acceleration, we require many different observational probes. The Integrated Sachs-Wolfe (ISW) effect (Sachs & Wolfe 1967) imprinted in the CMB and its correlation with the distribution of matter at lower redshifts is one such probe. The ISW effect arises from the time-variation of scalar metric perturbations and offers a promising new way to infer cosmological constraints (e.g. Corasaniti et al. 2005; Pogosian et al. 2006). It is usually divided, in the literature, into an early ISW effect and a late ISW effect. The early effect is important only around recombination when anisotropies begin to grow and radiation energy density is still dynamically important. The late ISW effect originates, on the other hand, long after the onset of matter domination. It is to this latter effect that we refer to here as the ISW effect. The origin of the late ISW effect lies in the time variation of the gravitational potential (e.g. Kofman & Starobinsky 1985; Kamionkowski & Spergel 1994). In a flat universe, the differential redshift of photons climbing in and out of the potential is zero except in a low matter density universe and at the onset of dark-energy domination.

The ISW effect is observed mainly in the lowest l-values range of the CMB temperature power spectrum ($l < 30$). It is import because it is sensitive to the amount, the equation of state, and the clustering properties of dark energy. Detection of such a weak signal is, however, limited by cosmic variance. Because the time evolution of the potential that gives rise to the ISW effect may also however be probed by observations of large-scale structure (LSS), the most effective way to detect the ISW effect is by means of the cross-correlation of the CMB with tracers of the LSS distribution. This idea, first proposed by Crittenden & Turok (1996), has been widely discussed in the literature (e.g. Kamionkowski 1996; Kinkhabwala & Kamionkowski 1999; Cooray 2002; Afshordi 2004; Hu & Scranton 2004). A detection of the ISW effect was first attempted using the COBE data and radio sources or the X-ray background (Boughn et al. 1998; Boughn & Crittenden 2002) without much success. The recent WMAP data (Spergel et al. 2003, 2007) provide high-quality CMB measurements on large scales. They were used in combination with many LSS tracers to reassess the

ISW detection. The correlations were calculated using data from various galaxy surveys (2MASS, SDSS, NVSS, APM, HEAO). However, despite numerous attempts in real space (Diego et al. 2003; Boughn & Crittenden 2004; Cabre et al. 2006; Fosalba & Gaztanaga 2004; Hernandez-Monteagudo & Rubiono-Martin 2004; Nolta et al. 2004; Afshordi et al. 2004; Padmanabhan et al. 2005; Gaztanaga et al. 2006; Giannantonio et al. 2006; Rassat et al. 2006), or in the wavelet domain (e.g. Vielva et al. 2006; McEwen et al. 2007), the ISW effect is detected by means of correlations with only weak significance. But the CMB and LSS surveys are now entering a precision age when they can start contributing to a stronger ISW detection, and hence provide valuable cosmological information, in particular about dark energy.

We explore the power of next generation CMB and LSS surveys in constraining the nature of dark energy through the cross-correlation of the ISW effect and the galaxy distribution. We start by using a signal-to-noise analysis to find the most appropriate properties of a survey that enable detection of correlated signal at a minimum significance level of 4σ. We then investigate the potential of a next generation experiments, obeying the aforementioned characteristics, to constrain different dark-energy models.

In Sect. 2, we revise the auto- and the cross-correlation angular power spectra of the ISW and of the galaxy distributions, and model the different contributions that enter the analysis. In Sect. 3, we focus on the signal-to-noise analysis that enables the optimisation of the galaxy survey data to provide an ISW detection. We quantify the requirements for an optimal next-generation survey planned within the context of the Cosmic Vision call for proposals, namely the DUNE mission (Refregier et al. 2006, `http://www.dune-mission.net/`). In Sect. 4, we present a Fisher analysis to determine the future constraints on the dark-energy equation of state through the correlation between CMB and LSS surveys. Finally we discuss the results and give our conclusions in Sect. 5.

2. Correlating the ISW effect and galaxy surveys

The ISW effect is a contribution to the CMB temperature anisotropies that arises in the direction $\hat{n}$ due to variations of the gravitational potential, Φ, along the path of CMB photons from last scattering until now,

$$\frac{\Delta T_{\rm ISW}}{T}(\hat{n}) = -2\int_0^{r_0} {\rm d}r\,\dot{\Phi}(r,\hat{n}r) \tag{1}$$

where $\dot{\Phi} \equiv \partial\Phi/\partial r$ can be conveniently related to the matter density field δ through the Poisson equation, assuming that the dark-energy component does not cluster (for an example of a clustering model see e.g. Weller & Lewis 2003). We set $c = 1$ here and in the following. The variable r is the conformal distance (or equivalently conformal time), defined today as r_0, and given by

$$r(z) = \int_0^z \frac{{\rm d}z'}{H_0 E(z')} \tag{2}$$

where, for a ΛCDM cosmology, $E(z)^2 \equiv \Omega_{\rm m}(1+z)^3 + \Omega_{\rm K}(1+z)^2 + \Omega_\Lambda$ with $\Omega_{\rm M}$, $\Omega_{\rm K}$ and Ω_Λ which correspond to the energy-density contributions of the matter, the curvature, and the cosmological constant today in units of the critical density, and H_0 is the present-day Hubble constant. If the dark energy is described by a quintessence field with a present energy density $\Omega_{\rm DE}$ and equation of state $w(z)$, then Ω_Λ in $E(z)$ is replaced by $\Omega_{\rm DE}(1+z)^3 \exp\left[3\int_0^z {\rm d}z'\, w(z')/(1+z')\right]$.

In a flat universe ($\Omega_{\rm K} = 0$), within the linear regime of fluctuations, the gravitational potential does not change in time if the expansion of the universe is dominated by a fluid with a constant equation of state. Therefore, for most of the time since last scattering, matter domination ensured a vanishing ISW contribution. Conversely, however, a detection of an ISW effect would indicate that the effective equation of state of the universe has changed. This is interesting, in particular, in the contest of the dark-energy dominated era.

Since the temperature of the CMB photons is modified, in the dark-energy dominated regime, as they traverse an over-density, the most effective way to detect the ISW effect is by means of its cross-correlation with the large-scale structure distribution. We therefore present the formalism used for computing the cross-correlation, in addition to the auto-correlation signal for both galaxies and CMB. It is noteworthy that the temperature change due to the gravitational redshifting of photons in the ISW is frequency independent and cannot be separated from the primary anisotropies using spectral information only.

By expanding the ISW temperature fluctuations in the sky in spherical harmonics, it is straightforward to show that the angular power spectrum of the ISW effect is given by (see e.g. Cooray 2002)

$$C_l^{\rm ISW} = \frac{2}{\pi}\int {\rm d}k\, k^2 P_{\delta\delta}(k)\left[I_l^{\rm ISW}(k)\right]^2, \tag{3}$$

where $P_{\delta\delta}(k)$ is the power spectrum of density fluctuations today, and

$$I_l^{\rm ISW}(k) = \int_0^{r_0} {\rm d}r\, W^{\rm ISW}(k,r) j_l(kr). \tag{4}$$

The ISW window function, in the case of a spatially-flat Universe with non-clustering dark energy, is

$$W^{\rm ISW}(k,r) = -3\Omega_{\rm M}\left(\frac{H_0}{k}\right)^2 \dot{F}(r). \tag{5}$$

The j_l are spherical Bessel functions of the first kind and $F(r) \equiv G(r)/a$ is the linear over-density growth factor G, divided by the scale factor a. G relates the density field δ, at any redshift, with its present-day value as $\delta(k,r) = G(r)\delta(k, r=0)$ and, for a ΛCDM cosmology, is given as a function of redshift by (see Heath 1977; Eisenstein 1997)

$$G(z) \propto \Omega_{\rm M} E(z)\int_z^\infty {\rm d}z'\,\frac{1+z'}{E^3(z')}\,. \tag{6}$$

It is normalized such that $G(z=0) = 1$. In the following, we use the Linder approximation for the growth factor (Linder 2005), which is given by

$$G(z) \propto \exp\left\{\int_\infty^z \left[\Omega_{\rm m}(z')^\gamma - 1\right]\frac{{\rm d}z'}{1+z'}\right\}, \tag{7}$$

where $\Omega_{\rm M}(z) = \Omega_{\rm M}\frac{(1+z)^3}{E(z)^2}$, and γ is a parameter set to 0.55 for the ΛCDM model. More generally, $\gamma = 0.55 + 0.05[1+w(z=1)]$ for an equation of state $w > -1$, and $\gamma = 0.55 + 0.02[1+w(z=1)]$ for $w < -1$. Equation (7) was shown to be a good approximation to the growth factor for dark-energy models with both a constant and a varying equation of state; it also approximates well the growth factor in modified-gravity models (e.g. Linder 2005; Amendola et al. 2007; Huterer & Linder 2007, and references therein).

We consider three paramerisations (A, B, and C) of w, as shown in Fig. 2:

- (A) constant equation of state: $w = -1$ (A1, i.e. the ΛCDM model) and $w = -0.9$ (A2);
- (B) linear evolution with the scale factor: $w(z) = w_0 + w_a \frac{z}{1+z}$;
- (C) kink parametrisation, where the equation of state undergoes a rapid transition at a particular redshift z_t: $w(z) = \frac{1}{2}(w_i + w_\infty) - \frac{1}{2}(w_i - w_\infty)\tanh\left(\Gamma \log\left(\frac{1+z_t}{1+z}\right)\right)$. w_i and w_∞ are the two assymptotic values (Douspis et al. 2006; Pogosian et al. 2006; Corasaniti et al. 2004).

These three parametrisations correspond to three different structure-formation histories. The respective growth-factor evolution, a key ingredient of the ISW effect as shown by Eq. (5), is presented in the bottom panel of Fig. 2.

Referring to Eq. (3), we defined the power spectrum of density fluctuations by $\langle\delta(\boldsymbol{k})\delta^*(\boldsymbol{k}')\rangle = (2\pi)^3\delta_D(\boldsymbol{k}+\boldsymbol{k}')P_{\delta\delta}(k)$ where

$$P_{\delta\delta}(k) \propto 2\pi^2\left(\frac{k}{H_0}\right)^{n_s+3}\frac{\mathcal{T}^2(k)}{k^3}, \tag{8}$$

with scalar spectral index n_s. The wavenumber k is expressed throughout in units of $h\,\mathrm{Mpc}^{-1}$. We use $H_0^{-1} = 2997.9\,h^{-1}\,\mathrm{Mpc}$ to represent the Hubble distance today. For the transfer function $\mathcal{T}$, we utilise the fitting formulae provided by Eisenstein & Hu (1997) for an arbitrary CDM+baryon universe. We use the proportionality symbol in the previous equation because the power spectrum is normalized on small angular scales to the cluster abundances that determine the parameter σ_8, the variance in the mass enclosed in spheres of radius $R = 8\,h^{-1}\,\mathrm{Mpc}$. In terms of the power spectrum, we have $\sigma_R^2 = 1/(2\pi)^2\int k^2 \mathrm{d}k P_{\delta\delta}(k)[3H_0 j_1(kR/H_0)/kR]^2$ (see e.g. Jaffe & Kamionkowski 1998).

Since we are interested in the cross-correlation of the CMB and galaxy distribution using data from large surveys, we define, in a similar manner, the two-point angular cross-correlation of the ISW temperature anisotropies with the galaxy-distribution field, given by

$$C_l^{\mathrm{ISW-G}} = \frac{2}{\pi}\int \mathrm{d}k\, k^2 P_{\delta\delta}(k) I_l^{\mathrm{ISW}}(k) I_l^{\mathrm{G}}(k), \tag{9}$$

where

$$I_l^{\mathrm{G}}(k) = \int_0^{r_0} \mathrm{d}r\, W^{\mathrm{G}}(k,r) j_l(kr), \tag{10}$$

and the galaxy window-function is given by

$$W^{\mathrm{G}}(k,r) = b_{\mathrm{G}}(k,r) n_{\mathrm{G}}(r) G(r). \tag{11}$$

In principle, $b_{\mathrm{G}}(k,r)$ is the scale- and redshift-dependent bias of the galaxies that we consider, and $n_{\mathrm{G}}(z) = n_{\mathrm{G}}(r)/H(z)$ is their normalised redshift-distribution defined by

$$n_{\mathrm{G}}(z) = n_{\mathrm{G}}^0\left(\frac{z}{z_0}\right)^\alpha \exp\left[-\left(\frac{z}{z_0}\right)^\beta\right], \tag{12}$$

where the variables α and β provide a description of the galaxy distribution, at low and at high redshifts, respectively, and z_0 corresponds to the median redshift $z_{\mathrm{med}} \simeq 1.4\,z_0$. The variable n_{G}^0 is a normalization such that $\int_0^{r_0} n_{\mathrm{G}}(r)\mathrm{d}r = 1$.

Examples of the angular power spectrum of the cross-correlation of the CMB with the galaxy distribution in large surveys are shown in Fig. 1, for the different cosmologies of Table 1. In our analysis, we neglect both the presence of massive neutrinos (cf. Lesgourgues et al. 2008) and magnification effects, which are more relevant at very high redshift (cf. LoVerde et al. 2007).

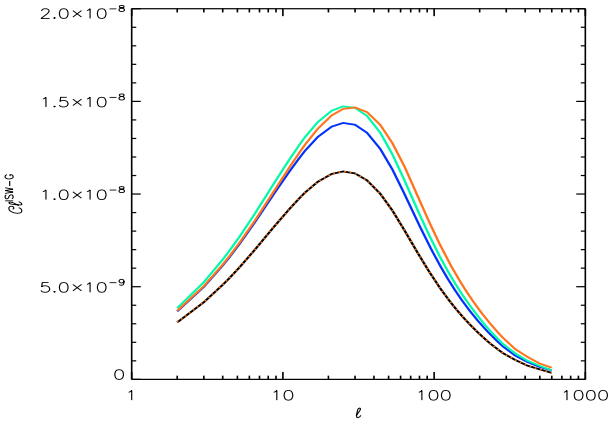

Fig. 1. The angular power spectrum of the correlation between LSS and CMB signals is shown for different cosmologies (see Table 1 for details). The ΛCDM model is shown in black, model A2 in dark blue, model B in green, model C with a transition at $a_t = 0.5$ ($a_t = 0.2$) in red solid (dotted) line.

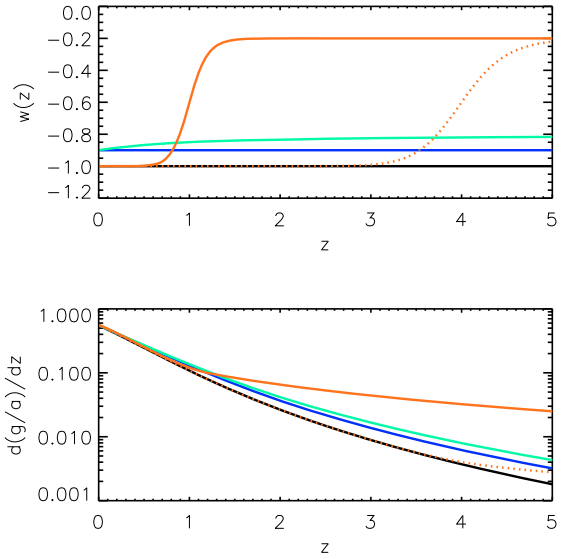

Fig. 2. *Top*: dark-energy equation of state, following parametrisation A1 (black), A2 (blue), B (green) and C (red) with the cosmological parameters given in Table 1. The dotted line corresponds to a parametrisation C with $a_t = 0.2$; *bottom*: corresponding $\dot{F}(z)$ (cf. Eq. (5)).

3. Signal-to-noise analysis

We start by investigating the detection level of the ISW effect in cross-correlation. To do this, we perform a signal-to-noise (SN) analysis. Using the power spectra computed in the previous section, we write the total signal-to-noise of the ISW detection as (Cooray 2002; Afshordi 2004):

$$\left(\frac{S}{N}\right)^2 = f_{\mathrm{sky}}^{\mathrm{c}}\sum_{l=l_{\mathrm{min}}}^{l_{\mathrm{max}}}(2l+1) \times \frac{\left[C_l^{\mathrm{ISW-G}}\right]^2}{\left[C_l^{\mathrm{ISW-G}}\right]^2 + \left(C_l^{\mathrm{ISW}} + N_l^{\mathrm{ISW}}\right)\left(C_l^{\mathrm{G}} + N_l^{\mathrm{G}}\right)}, \tag{13}$$

Table 1. Values of cosmological parameters for the fiducial models used in the Fisher analysis. Note that we impose flatness for all models.

Model	H_0	Ω_b	Ω_M	σ_8	n_s	w_0	w_a	a_t
A1	73	0.04	0.24	0.74	0.951	–1	–	–
A2	73	0.04	0.24	0.74	0.951	–0.9	–	–
B	73	0.04	0.24	0.74	0.951	–0.9	0.1	–
C	73	0.04	0.24	0.74	0.951	–	–	0.5

Table 2. Future LSS surveys characteristics (1) from Refregier et al. (2006, 2008) and the DUNE website; (2) and (3) from Pogosian et al. (2005) as "conservative" and "goal" cases respectively; (4) from the SNAP collaboration, the SNAP website http://snap.lbl.gov/ and Aldering et al. (2007); (5) from Stubbs et al. (2007), Heavens et al. (2007), and private communications with Phleps. Planck characteristics used for the noise part of the signal-to-noise, and for the Fisher matrices analyses are also given. The values of z_{med} for SNAP and $\bar{N}$ for PanSTARRS are only indicative.

	f_{sky}	z_{med}	nbar (arcmin^{-2})
DUNE(1)	49%	0.9	40
LSST-1(2)	30%	1	50
LSST-2(3)	49%	1.8	70
SNAP(4)	1 %	1.8	100
PanSTARRS(5)	50%	0.75	5
PLANCK	$f_{sky} = 80\%$	$\theta_{beam} = 7$ arcmin	$\omega_T^{-1} = 4e^{-17}$

where f_{sky}^c is the fraction of sky common to both the CMB and the galaxy survey maps, and the total (or cumulative) signal-to-noise is summed over multipoles between $l_{min} = 2$ and $l_{max} = 60$, where the signal has its major contribution. The spectra C_l^{ISW-G} and C_l^{ISW} were defined in the previous section, and C_l^G is straightforward to obtain. The noise contribution in the ISW signal and galaxy surveys are N_l^{ISW} and N_l^G, respectively. On the scales of interest for the ISW detection, and for the CMB experiment considered, the ISW noise is defined to be $N_l^{ISW} = C_l^{CMB} + N_l^{CMBexp}$, where N_l^{CMBexp} is the contribution from the experimental noise. The previous expression is dominated by the sample variance. However, we include N_l^{CMBexp} in our calculations, as modeled in Knox (1995), for an experiment such as the Planck satellite (see Table 2 for the CMB noise characteristics). The galaxy-survey noise is defined by the shot-noise contribution: $N_l^G = \frac{1}{\bar{N}}$ where $\bar{N}$ is the surface density of sources per steradian that one can effectively use for the correlation with CMB temperature data. The noise part of the SN depends then, to first order, on the common sky fraction, the surface density of sources, and the median redshift of the sources through the amplitude of the cross-power spectrum C_l^{ISW-G} and the galaxy auto-correlation signal C_l^G. With this analysis, we are then able to optimise our analysis of data from forthcoming galaxy surveys to search for an ISW detection in cross-correlation as a function of their three main parameters namely z_{med}, f_{sky}^c and $\bar{N}$. We use the cosmological parameter values from WMAP3 (Spergel et al. 2007) as listed in Table 1.

We explore the 3D parameter space, and in Figs. 3–5, show the SN values in 2D diagrams where we marginalised over the third parameter, $\bar{N}$ for the left panel and z_{med} for the right panel, respectively. To obtain an insight into the detection level of the ISW, we computed the SN values for the dark-energy models A and B given in Sect. 2. We did not consider the kink parametrisation (model C) because it provides similar results to linear parametrisation. All the results shown in this section were

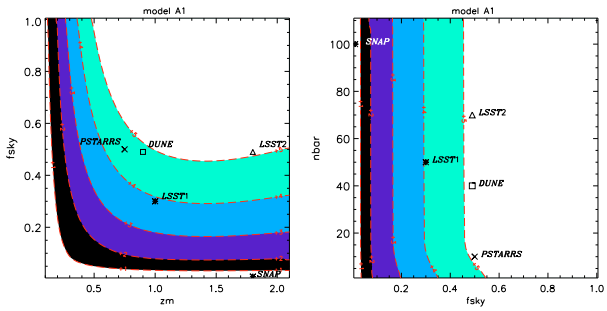

Fig. 3. Total signal-to-noise for a ISW detection in the ΛCDM model (parametrisation A1) as a function of the galaxy survey parameters f_{sky}^c, $\bar{N}$ in units of arcmin^{-2} and z_{med}. The different colours show different levels of detection in number of sigmas.

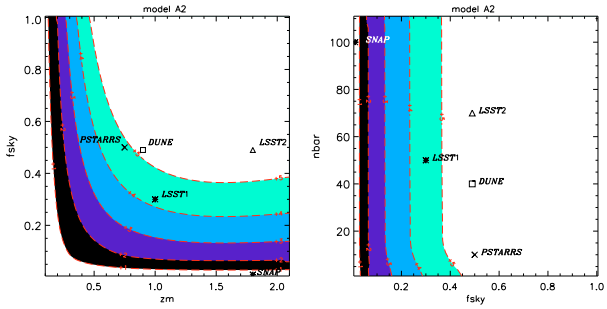

Fig. 4. Total signal-to-noise for a ISW detection in the constant equation of state model with $w = -0.9$ (parametrisation A2) as function of the galaxy survey parameters f_{sky}^c, $\bar{N}$ in units of arcmin^{-2} and z_{med}.

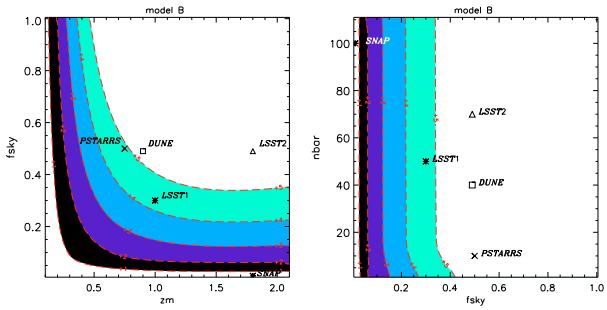

Fig. 5. Total signal-to-noise for a ISW detection in the linearly varying equation of state model (parametrisation B) as function of the galaxy survey parameters f_{sky}^c, $\bar{N}$ in units of arcmin^{-2} and z_{med}.

obtained using a redshift and scale independent bias $b_G = 1$, and using the parameters $\alpha = 2$ and $\beta = 1.5$, for the galaxy redshift distribution. This set of parameters is typical for optical galaxy studies (Heavens et al. 2007).

From all these figures, we can see that once the number density of observed sources $\bar{N}$ reaches a given value $\bar{N}_{lim}$, which is typically about 10 sources per arcmin^2 or a bit less for all dark-energy models, the SN is constant and independent of $\bar{N}$. This can be understood by going back to the definition of the survey noise (N_l^G) provided by the SN ratio equation (Eq. (13)): in this regime, the contribution from the Poisson noise becomes negligible. As a result, for an equal sky fraction f_{sky}^c and median redshift z_{med}, all surveys satisfying the condition $\bar{N} > \bar{N}_{lim}$ provide equivalent ISW detections. At a fixed $\bar{N} > \bar{N}_{lim}$, the SN ratio is, in contrast, very sensitive to f_{sky}^c and z_{med}.

Conversely, increasing z_{med} at a given f_{sky}^c, improves significantly the ISW detection only up to $z_{med} \sim 1$. In the chosen

dark-energy model, dark energy domination always occurs for $z < 1$.

In the ΛCDM model, a detection of the ISW signal at a confidence level of 4σ is attained for median redshifts $z_{\rm med} > 0.84$ and fractions of sky $f_{\rm sky}^{\rm c} > 0.35$. For a constant equation of state model ($w = -0.9$), we find a slightly lower median redshift, of ∼0.8, and a slightly lower sky fraction $f_{\rm sky}^{\rm c} \sim 0.33$, and similar numbers apply for the varying equation of state model. The small increase in SN for models A2 and B is expected, since the ISW is an integrated effect. In the last two models, dark-energy domination occurs earlier, and structures grow faster. Therefore, they provide a stronger contribution to the ISW effect than ΛCDM, ensuring higher SN for lower median redshift.

We conclude that, for the dark-energy models considered here, to ensure detection of the ISW effect using cross-correlation methods and data of sufficiently high signal-to-noise ratio, it is important to design a galaxy survey using predictions of the ΛCDM model. The ΛCDM model gives, in fact, the most conservative detection levels. An optimal survey, with a detection level above 4σ, should thus be designed so that it has a minimum number density of sources of about around 10 galaxy per arcmin^{-2}, covers a sky fraction of at least 0.35 and is reasonably deep, with a minimum median redshift larger than 0.8. One of the surveys satisfying such conditions and being planned is the DUNE mission proposed to the ESA's Cosmic Vision call for proposal (Refregier et al. 2006, 2008, http://www.dune-mission.net/). It will provide detection at a significance level of almost 5σ, as shown in Figs. 3–5, in addition to other future galaxy surveys such as SNAP, PanSTARRS and LSST; see Table 2.

4. Fisher matrix analysis

We perform a Fisher matrix analysis to quantify the constraint on dark energy that a cross-correlation with CMB maps of a next-generation large-scale survey, would provide by means of the ISW signal. For the ISW measurement, such an analytical approach has been shown by Cabré et al. (2007) to yield similarly reliable error bars as full realistic Monte-Carlo simulations of CMB and galaxy maps. We use this technique to compute the errors on a set of cosmological parameters Θ. We assume the usual experimental characteristics, such as the noise and the sky fraction, of Planck and DUNE surveys, as listed in Table 2, because these are excellent examples of the next generation of CMB and LSS experiments. They ensure a good SN detection as demonstrated in the previous section.

Given the characteristics of the CMB and the LSS experiments, a fiducial model, and a cosmological framework, the smallest possible errors on a set of parameters when determined jointly were shown to be given by the Fisher matrix F elements: $\delta\Theta_i = \sqrt{(F^{-1})_{ii}}$ (see e.g. Tegmark et al. 1997). In our case, the cross-correlation Fisher matrix for parameters Θ_i and Θ_j is given by

$$F^{i,j} = f_{\rm sky}^{\rm c} \sum_l (2l+1) \frac{\partial C_l^{\rm ISW-G}}{\partial \Theta_i} \, {\rm cov}^{-1}(l) \, \frac{\partial C_l^{\rm ISW-G}}{\partial \Theta_j} \qquad (14)$$

where

$${\rm cov}(l) = \left[C_l^{\rm ISW-G}\right]^2 + \left(C_l^{\rm ISW} + N_l^{\rm CMB}\right)\left(C_l^{\rm G} + N_l^{\rm G}\right). \qquad (15)$$

The summation is completed over the range of multipoles for which the partial derivatives of the C_ℓ's are significant ($\sim\pi/(2f_{\rm sky}^{\rm c}) < l < 800$). The covariance term, in addition to the partial derivatives, are evaluated at the fiducial model; in Sect. 3 (Eq. (13)) we provide more details about the various terms entering the expression.

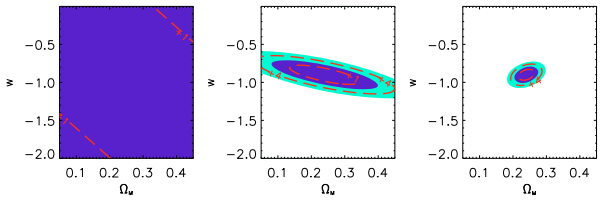

Fig. 6. Two-dimensional marginalised confidence intervals on the plane $(\Omega_{\rm M}, w)$ obtained with a Fisher matrix analysis centred on model A2 with $w = -0.9$. *Left*: ISW constraints; center: CMB (temperature) constraints; *right*: combined constraints (see text for details).

We assume a flat universe with adiabatic scalar perturbations, a nearly scale invariant initial power spectrum, containing baryonic and cold dark matter, and dark energy. We assume zero curvature because, if it were not the case, dark energy would be indistinguishable from curvature using the ISW effect (Kunz 2007; Clarkson et al. 2007). The Fisher analysis is then completed using the following cosmological parameters: $\Theta = (H_0, \Omega_{\rm b}, \sigma_8, n_{\rm s}, \Omega_{\rm DE})$. With respect to the dark energy component, we study the three scenarios A, B, and C given in Sect. 2 and summarised in Table 1.

We compute the Fisher matrix that corresponds to the constraints imposed by the CMB alone for the same three scenarios. We take into account only one channel, in temperature, following the Planck characteristics listed in Table 2. When combining the constraints from the CMB alone and from the cross-correlation, we consider that the experiments are independent and thus add the corresponding Fisher matrices.

Figure 6 shows the constraints obtained from the Fisher analyses of model A2 with $w = -0.9$, from the cross-correlation between the CMB and the LSS (left), from the CMB temperature anisotropies alone (middle), and from the combined analysis of both (right). The panels show the confidence intervals that one could obtain for $\Omega_{\rm M}$ and w when other parameters are marginalised over. As shown in the figure, the constraints from the cross-correlation itself are quite weak, but they do not play an obvious or negligible role in the combination. This is mainly due to the 6-dimensional shape of the likelihood and its degeneracies.

To further investigate such a result, we added strong priors on some cosmological parameters to the cross-correlation Fisher matrix (instead of the CMB Fisher matrix). We found that adding a prior to the Hubble constant (H_0), the matter content ($\Omega_{\rm M}$), or the spectral index ($n_{\rm s}$) did not improve significantly the constraints. However, the errors of the dark energy parameters are significantly reduced when a prior is added to the amplitude of the fluctuations expressed in terms of σ_8. Figure 7 shows the constraints obtained from the cross-correlation in this last case for scenario A2 ($w = -0.9$) without (left plots) and with (right plots) a strong prior on σ_8, where $\sigma_8 = 0.7 \pm 0.02$. The top left panel shows the degeneracy between σ_8 and w and explains why, by constraining strongly σ_8, with a prior (right panel) or with the CMB (Fig. 6), the equation of state is determined more accurately. This and other minor degeneracy breakings in the 6-dimensional space enable the ISW effect, using cross-correlation, to improve the constraints on dark energy.

As shown previously, the CMB by itself is only able to constrain one parameter of the dark energy model, since it is

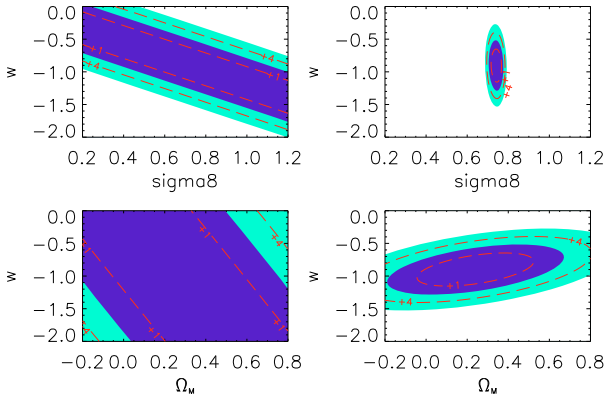

Fig. 7. Two-dimensional marginalised confidence intervals obtained with a Fisher matrix analysis centered on model A2 with $w = -0.9$ for different combinations of parameters: (Ω_M, w) and (σ_8, w). *Left*: ISW constraints; *right*: ISW constraints obtained with a strong prior on σ_8 (see text for details). Note that the scales for Ω_M are different from Fig. 6.

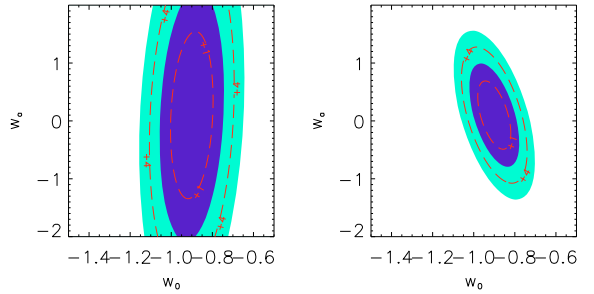

Fig. 8. Two-dimensional marginalized confidence intervals obtained with a Fisher matrix analysis for (w_0, w_a) centered on model B with $w(a) = -0.9 + 0.1(1 - a)$. *Left*: CMB (temperature) constraints; *right*: CMB+ISW combined constraints (see text for details).

sensitive mainly to the distance to the last-scattering surface (see e.g. Pogosian et al. 2006; Douspis et al. 2008, and references therein). Therefore, in scenario B with $w(a) = w_0 + (1 - a)w_a$, only the value of the equation of state at present w_0 is constrained (Fig. 8 left). The errors on the linear expansion factor w_a shown in the right panel of Fig. 8, are again improved slightly by information provided by the cross-corrrelation between Planck and DUNE data. However, it does not help to distinguish a constant and a linear dark energy model.

Finally, we study the "kink" model C to assess the sensitivity of the cross-correlation to probe a sharp transition in the evolution of w. The model considered shows a sharp transition ($\Gamma = 10$) between $w(z = 0) = -1$ and some arbitrary value close to 0 far in the past, e.g. $w(z = \infty) = -0.2$. We choose in this case, to allow the transition redshift z_t to vary because we can constrain only one dark energy parameter using the CMB. The equation of state is $w = -1$ for most of the period of structure formation, for transitions that occur sufficiently early in time. Little difference is then expected between such a model and a ΛCDM model (see Fig. 2). For recent transitions, in contrast, significant effects are expected. This model was studied by Douspis et al. (2008) using current CMB and SNIa data, which shows that a transition at $z_t > 0.5$ ($a_t < 0.66$) is allowed. The Fisher matrix analysis, which gives the smallest possible error bar on the parameters, relies by construction on the hypothesis of a Gaussian likelihood for the C_ℓ. This prevents asymmetric error

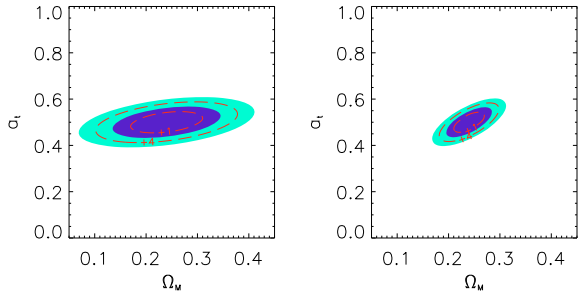

Fig. 9. Two-dimensional marginalized confidence intervals obtained with a Fisher matrix analysis centered for (Ω_M, a_t) on model C with $w(0) = -1$, $w(\infty) = -0.2$ and $a_t = 0.5$; *left*: CMB (temperature) constraints; *right*: combined constraints (see text for details).

bars on the parameters, and in this particular case does not allow us to obtain the realistic constraints that one could have: which means that transitions at $a_t < 0.4$ are also allowed. This can be seen by comparing Fig. 9 (left panel) with Fig. 5 of Douspis et al. (2008). We choose to take as reference model for scenario C (see Table 1) a reasonable value for the period of transition, $a_t = 0.5$. Due to the large difference of impact on the growth of structure as a function of a_t (see Fig. 2), the errors in the transition period are strongly dependent on the reference model chosen. In our case, we see in the right panel of Fig. 9 that adding the ISW information to the CMB temperature anisotropy improves the constraints on Ω_M in the plane (Ω_M, a_t), but does not improve constraints on a_t.

5. Conclusions

We have analysed the cross-correlation between the ISW effect and a galaxy survey characterised by the redshift distribution given by Eq. (12) and assuming simple Poisson noise. We rely on the Linder approximation given by Eq. (7) to model the growth of structure in dynamical dark energy models.

We determine the most appropriate properties of a survey to detect an ISW signal in cross-correlation CMB/LSS at a minimum of 4 sigma. We use a signal to noise analysis to achieve this aim. Our results agree with those obtained by Afshordi (2004): we show that the necessary properties for a survey to be significantly successful in the quest for an ISW signal are a minimum number density of sources of about 10 galaxies per arcmin^2, a minimum sky fraction of the order of 0.35 and a minimum median redshift of about 0.8. We indicate that the DUNE project is a promising candidate for providing a good ISW detection, once correlated with Planck data. Furthermore, the number of galaxies detected by such a survey is sufficiently high to divide the distribution into different redshift bins, allowing the dark energy to be probed at different epochs. We address the tomography in ISW studies in a following paper. As found above, the Poisson noise is negligible for a number of detected galaxies which is higher than 10 per arcmin^{-2}. If this condition is met in each redshift bin, this increases the signal to noise correspondingly to the number of bins considered.

We then investigate the power in constraining different dark energy models of typical next generation experiments having the aformentioned characteristics. We take the DUNE and the Planck surveys. Here again, we confirm the result of previous analyses, such as those of Pogosian et al. (2006) and Douspis et al. (2008). We show that the ISW effect does help, as compared to CMB alone, in breaking degeneracies among the

parameters describing the dark energy model and the other cosmological parameters, primarily σ_8. The cross-correlation allows us to put a constraint of the order of 10% on w for a model with a constant equation of state (A) and reduces the errors on the estimation of the parameter w_a in a linear model (B). However, it does not permit us to distinguish between a constant and a dynamical equation of state for the dark energy. Fitting a dark energy model with a kink, we find that adding the cross-correlation does not improve the CMB constraints on the transition redshift: the ISW is therefore insensitive to sharp transitions, and a transition at any redshift larger than 0.5 is still allowed.

Acknowledgements. N.A. and M.D. thank the collaboration programme PAI-PESSOA for partial funding. They further thank Instituto Superior Técnico (IST) for hospitality. PGC is funded by the *Fundação para a Ciência e a Tecnologia* and wishes to thank the Institut d'Astrophysique Spatiale (IAS) for its welcoming and support, and Stefanie Phleps for useful conversations. CC acknowledge support by the ANR funding PHYS@COL&COS, and thanks IAS and IST for hospitality. We thank Mathieu Langer for helpful comments.

References

Afshordi, N. 2004, Phys. Rev. D, 70, 083536
Afshordi, N., Loh, Y., & Strauss, M. A. 2004, Phys. Rev. D, 69, 083524
Aldering, G., Kim, A. G., Kowalski, M., Linder, E. V., & Perlmutter, S. 2007, Astropart. Phys., 27, 213
Amendola, L., Kunz, M. & Sapone, D. 2007 [arXiv:0704.2421]
Boughn, S. P., & Crittenden, R. G. 2002, Phys. Rev. Lett., 88, 021302
Boughn, S. P., & Crittenden, R. G. 2004, Nature , 427, 45
Boughn, S. P., Crittenden, R. G., & Turok, N. G. 1998, New Astron., 3, 275
Cabré, A., et al. 2007 [arXiv:astro-ph/0701393]
Cabré, A., Gaztañaga, E., Manera, M., Fosalba, P., & Castander, F. 2006, MNRAS, 372, L23
Clarkson, A., Cortês, M. & Bassett, B. 2007, J. Cosm. Astropart. Phys., 0708:011
Corasaniti, P., Kunz, M., Parkinson, D., Copeland, E. J., & Bassett, B. A. 2004, Phys. Rev. D, 70, 083006
Corasaniti, P., Gianantonio, T., & Melchiorri, M. 2005, Phys. Rev. D, 71, 123521
Cooray, A. 2002, Phys. Rev. D, 65, 103510
Crittenden, R. G., & Turok, N. G. 1996, Phys. Rev. Lett., 76, 575
Diego, J., Hansen, H., & Silk, S. 2003, MNRAS, 338, 796
Douspis, M., et al. 2008, A&A, accepted [arXiv:astro-ph/0602491]
Eisenstein, D. J. 1997 [arXiv:astro-ph/9709054]
Eisenstein, D. J., & Hu, W. 1998, ApJ, 496, 605
Fosalba, P., & Gaztanaga, E. 2004, MNRAS, 350, L37
Gaztanaga, E., Maneram, M., & Multamaki, T. 2006, MNRAS, 365, 171
Giannantonio, T., et al. 2006, Phys. Rev. D, 74, 063520
Heath, D. J. 1977, MNRAS, 179, 351
Heavens, A. F., Kitching, T. D., & Verde, L. 2007, [arXiv:astro-ph/0703191]
Hernandez-Monteagudo, C., & Rubino-Martin, J. A. 2004, MNRAS, 347, 403
Hu, W., & Scranton, R. 2004, Phys. Rev. D, 70, 123002
Huterer, D., & Linder, E. V. 2007, Phys. Rev. D, 75, 023519
Kamionkowski, M. 1996, Phys. Rev. D, 54, 4169
Kamionkowski, M., & Spergel, D. N. 1994, ApJ, 432, 7
Kinkhabwala, A. & Kamionkowski, M. 1999, Phys. Rev. Lett., 82, 4172
Knox, L. 1995, Phys. Rev. D, 52, 4307
Kofman, L. A., & Starobinsky, A.A. 1985, Soviet. Astron. Lett. (Tr: Pisma), 11, 5, 271
Kunz, M. 2007 [arXiv:astro-ph/0702615]
Jaffe, A. H., & Kamionkowski, M. 1998, Phys. Rev. D, 58, 043001
Lesgourgues, J., Valkenburg, W., & Gaztanaga, E. 2008, Phys. Rev. D, 77, 063505
LoVerde, M., Hui, L. & Gaztanaga, E. 2007, Phys. Rev. D, 75, 043519
Linder, E. V. 2005, Phys. Rev. D, 72, 043529
McEwen J. D., Vielva, P., Hobson, M. P., Martínez-González, E., & Lasenby, A. N. 2007, MNRAS, 376, 1211
Nolta, M. R., Wright, E. L., Page, L., et al. 2004, ApJ, 608, 10
Padmanabhan, N., Hirata, C.M., Seljak, U., et al. 2005, Phys. Rev. D, 72, 043525
Pogosian, L., Corasaniti, P. S., Stephan-Otto, C., Crittenden, R., & Nichol, R. 2005, Phys. Rev. D, 72, 103519
Rassat, A., Land, K., Lahav, O., & Abdalla, F. B. 2007, MNRAS, 377, 1085
Refregier, A., et al. 2006 [arXiv:astro-ph/0610062]
Refregier, A., et al. 2008, Experimental Astronomy, submitted
Sachs, R. K., & Wolfe, A. M. 1967, ApJ, 147, 73
SNAP Collaboration, Albert, J., et al. 2005, SLAC-PUB-11393
Spergel, D. N., Verde, L., Peiris, H. V., et al. 2003, ApJS, 148, 175
Spergel, D. N., Bean, R., Doré, O., et al. 2007, ApJS, 170, 377
Stubbs, C. W., High, F. W., George, M. R., et al. 2007, Publ. Astron. Soc. Pac., C119, 1163
Tegmark, M., Taylor, A., & Heavens, A. 1997, ApJ, 480, 22
Tyson, J. A. for the LSST Collaboration 2006 [arXiv:astro-ph/0609516]
Vielva, P., Martinez-Gonzalez, E., & Tucci, M. 2006, MNRAS, 365, 891
Weller, J., & Lewis, A. 2003, MNRAS, 346, 987